Identification of the discharge kinetics in the perfluoro-nitrile C4F7N with swarm and breakdown experiments

Journal Article

Author(s):
Hösl, Andreas (iD); Chachereau, Alise (iD); Pachin, Juriy (iD); Franck, Christian (iD)

This is the post-review version of the article submitted to J.PhysD (https://dx.doi.org/10.1088/1361-6463/ab0f45), published on 27.03.2019.

Identification of the discharge kinetics in the perfluoro-nitrile C_4F_7N with swarm and breakdown experiments

Andreas Hösl[ID]**, Alise Chachereau**[ID]**, Juriy Pachin**[ID]**, Christian M. Franck**[ID]

Power Systems and High Voltage Laboratories, ETH Zurich, Physikstr. 3, 8092 Zurich, Switzerland

E-mail: `cfranck@ethz.ch`

Abstract. We follow up on our previous publication on C_4F_7N and investigate the ion kinetics influencing C_4F_7N discharges with a pulsed Townsend experiment. The measured current signals at pressures between 0.06 and 6.9 kPa, in the range of density-reduced electric fields E/N from 500 to 1050 Td, show evidence of three anions: one long-lived anion with a detachment rate coefficient in the order of $10^{-20} \mathrm{m^3 s^{-1}}$, a presumably non-detaching anion, and a short-lived anion with a detachment rate coefficient in the order of $10^{-17} \mathrm{m^3 s^{-1}}$. We obtain the corresponding rate coefficients for ionization, attachment and detachment in C_4F_7N. Using these results, we calculate a corrected value of the effective ionization rate coefficient $(\nu_{\mathrm{eff}}/N)^*$, taking into account detachment from negative ions. It results in a corrected value of the density-reduced critical electric field strength $(E/N)^*_{\mathrm{crit}} = 785 \pm 15$ Td, much lower than the previously obtained value of $(E/N)_{\mathrm{crit}} = 975 \pm 15$ Td, which is valid only when electron detachment is negligible, i.e. for low pressure and small geometric distance. To find which value is most relevant for electrical insulation, we perform breakdown voltage measurements in homogeneous electric fields in C_4F_7N at 5 to 65 kPa. We compare the measured density-reduced breakdown field strength $(E/N)_{\mathrm{bd}}$ to that calculated using the streamer criterion with the presently obtained rate coefficients, including electron detachment. We find excellent agreement between the measured and calculated $(E/N)_{\mathrm{bd}}$.

Introduction

We investigate the electron and ion kinetics driving electrical discharges in the perfluorinated nitrile $(CF_3)_2CFC\equiv N$, which we refer to in the following as C_4F_7N. This compound has been proposed as an environment-friendly alternative to SF_6 in high voltage gaseous electrical insulation [1, 2], due to its lower global warming potential compared to SF_6.

The AC breakdown voltage of C_4F_7N in uniform electric field was the object of a few publications. We discuss the results in terms of density-reduced breakdown field strength $(E/N)_{\mathrm{bd}}$.

Owens compared the breakdown strength of C_4F_7N and SF_6 in an arrangement of "relatively uniform field", and claims a superior strength of C_4F_7N by a factor of ≈ 1.9 [3]. However, his breakdown strength in SF_6 corresponds to $(E/N)_{\mathrm{bd}} \approx 244$ Td at 100 kPa (1 bar) and $(E/N)_{\mathrm{bd}} \approx 122$ Td at 600 kPa, and thus is strongly dependent on pressure and far from the commonly accepted value of the density-reduced critical electric field $(E/N)_{\mathrm{crit}} = 360$ Td [4].

Nechmi et al. [5] extrapolate a breakdown strength in homogeneous fields of 982 Td, which fits comparably well with our findings. Zhang et al. find, for pure C_4F_7N in homogeneous fields, a value of ≈ 800 Td at 100 kPa, dropping to 620 Td at 200 kPa [6]. They further state a field strength in SF_6 of ≈ 330 Td at 100 kPa and ≈ 270 Td at 200 kPa. Other works focus on the breakdown voltage of C_4F_7N mixtures rather than pure C_4F_7N [7, 8, 9].

In a previous publication [10], we presented a preliminary analysis of the electron swarm parameters in C_4F_7N using a pulsed Townsend experiment, and found that the critical electric field of C_4F_7N is 975 ± 15 Td at low pressures and small geometric distance, where electron detachment is negligible. Furthermore, we showed that ion current dynamics, and in particular electron detachment from negative ions influence the discharge to a large extent at gas pressures above 0.1 kPa, and therefore presumably also the electrical insulation performance. The reason for this is that electron detachment from ions impairs their capability of removing electrons from an avalanche, and therefore lowers the electric strength of the compound compared to the non-detaching case; this is for instance discussed in detail in [11].

In the present work, we complement the pulsed Townsend measurements from our previous work with additional measurements in pure C_4F_7N at pressures up to 6.9 kPa. We propose a kinetic model including three negative ion species to describe the discharges in pure C_4F_7N, and use this model to re-evaluate our previous measurements together with the new measurements. We obtain the rate coefficients of attachment and detachment for all dominant anions as well as the ionization rate coefficient. This allows us to calculate the corrected values of the effective ionization rate coefficient $(\nu_{\mathrm{eff}}/N)^*$ and density-reduced critical electric field strength $(E/N)^*_{\mathrm{crit}}$.

In addition, we perform AC breakdown voltage measurements in uniform electric field in C_4F_7N. In order to compare both results, we simulate the avalanche

in a uniform field configuration and apply an adapted "streamer criterion", analogous to the criterion in non-detaching gases. This then yields an estimate for the density-reduced breakdown field strength $(E/N)_{bd}$ of C_4F_7N.

This work is structured as follows. The experimental setting of the pulsed Townsend experiment and the breakdown experiment is described briefly. We review the optimization procedure for fitting the current waveforms measured with the pulsed Townsend experiment with the chosen kinetic model, and discuss the choice of the model. We then present these results: ion mobilities, ionization, attachment and detachment rate coefficients, effective ionization coefficient and critical electric field. Finally we show the results of the breakdown experiment, compared to calculations made with an adapted streamer criterion using the rate coefficients from the pulsed Townsend experiment.

1. Experimental methods

1.1. Pulsed Townsend experiment

The Pulsed Townsend setup consists of two electrodes of variable distance which span a homogeneous electric field. A pulsed UV source of 266 nm wavelength, pulse width of 1.5 ns, 20 Hz and 200 μJ pulse energy illuminates a photocathode from the back, which is a quartz coated with 15 nm of magnesium and 5 nm of palladium. The pulse releases $10^4 - 10^7$ electrons, which travel $1 - 3$ cm in an homogeneous field towards the anode and interact with neutral gas molecules. The superimposed displacement current of electrons, positive and negative ions is measured. For details about the experimental setup and measurement conditions we refer to our previous publication [10].

We evaluate multiple measurements in pure C_4F_7N, including the measurements presented in [10]. Our measurements cover a pressure range from 0.060 kPa up to 6.9 kPa. The measurements below 2 kPa were measured in an (E/N) range of $700 - 1050$ Td. For the measurements above 2 kPa, we are able to extend the (E/N) range down to 500 Td, but are limited to 950 Td due to impending breakdown. This already gives an indication that the critical electric field strength $(E/N)_{crit}$ of 975 Td from [10], obtained by considering ionization and attachment alone, overestimates the electric strength. Most measurements were recorded on the Pulsed Townsend experiment described in [12]. The measurements with pressures above 2 kPa were recorded on the older experiment [13].

1.2. Breakdown experiment

The breakdown experiments were performed using the setup described in [14]. An homogeneous field (50 Hz AC) is applied between two Rogowski-shaped stainless steel (EN 1.4460) electrodes of 80 mm diameter and flat area of 40 mm. For the results of this publication the electrode spacing was kept at 15 mm (unless otherwise noted). The parallelity of the electrodes is ensured to be better than few 10 μm with adjustment screws. Taking into account thermal expansion of the materials and mechanical accuracy, the electrode spacing accuracy is estimated as 100 μm.

Two kinds of electrode surfaces were used: one polished with a roughness of $R_a = 0.04$ μm and $R_t = 1.3$ μm; and one sandblasted with a roughness of $R_a = 2 - 4$ μm and $R_t = 13$ μm. The electrodes were frequently cleaned after few hundred breakdowns, due to substantial soot deposition. In order to increase the availability of free electrons, we also perform separate measurement series with UV irradiation (254 nm) of the electrodes.

The voltage increase rate is 2 kV/s till 90% of the presumed breakdown strength is reached, and then $0.1 - 0.2$ kV/s. We try also $0.01 - 0.02$ kV/s. The (peak) voltage measurement uncertainty is 2%, and temperature is determined to $\pm 1°$C. The accuracy of the calibrated pressure gauge is 0.25%. Before filling, the vessel is evacuated to below 10 Pa. To avoid contamination, separate glass-fiber reinforced epoxy vessel are used for different gases.

For each breakdown measurement series 40 to 125 individual breakdowns are performed. Dependant on the breakdown voltage and the voltage increasing rate two to ten minutes were kept in between the individual breakdowns. We append measurements of the well-known gases SF_6 and N_2 (the latter from [14]) as reference for this setup.

2. Fitting procedure

The fitting method is described in detail in [15], where we developed it and applied it to synthetic air. A finite-volume simulation is used to simulate the transport of electrons and ions in a homogeneous electric field, for arbitrary linear models. Then, starting with a random guess of rates, an optimization procedure is used to find an overlap between the measured and simulated currents. Since this process requires thousands of simulations, we use GPUs to provide the necessary computational resources.
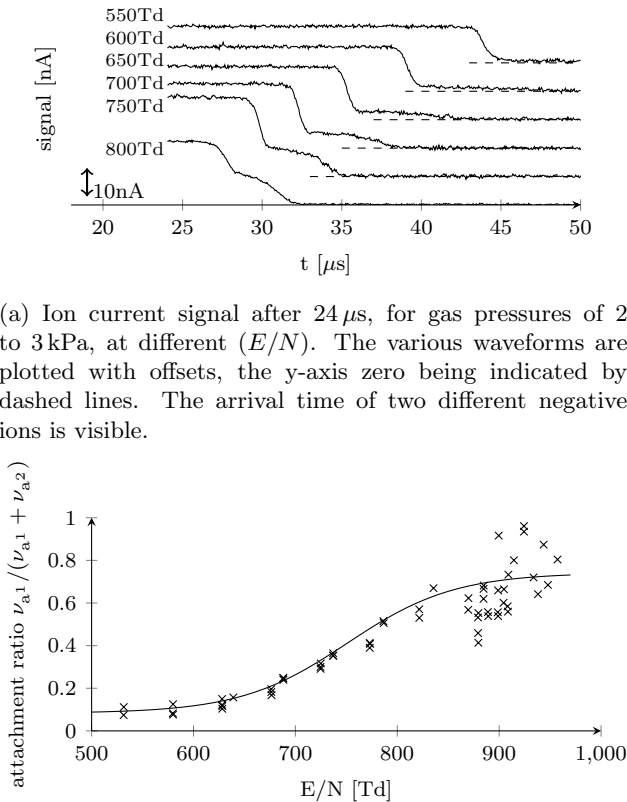
(a) Ion current signal after $24\,\mu$s, for gas pressures of 2 to $3\,$kPa, at different (E/N). The various waveforms are plotted with offsets, the y-axis zero being indicated by dashed lines. The arrival time of two different negative ions is visible.
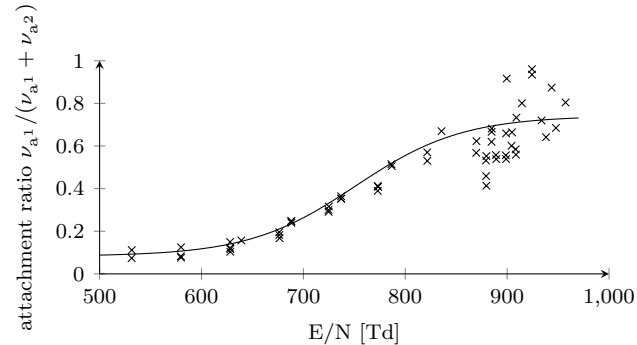
(b) Ratio of the attachment rates $\nu_{a^1}/(\nu_{a^1}+\nu_{a^2})$ of the long-lived anions M_1^- and M_2^-, matching the observed increase in the slower anion M_1^- with increasing (E/N) of figure 1a. Obtained from measurements at pressures of $2-7\,$kPa.

Figure 1

3. Kinetic model

3.1. Evidence for two long-lived anions M_1^- and M_2^-

Figure 1a shows the current waveforms measured at different (E/N) from 500 to $800\,$Td, for gas pressures of $2-3\,$kPa. At these relatively low (E/N) values and at the considered pressure, all the released electrons from the photocathode are immediately (i.e. within few ns, not observable with our setup and omitted in the figure) attached to negative ions, which drift towards the anode. All ions of one anion species with a specific drift velocity will arrive almost simultaneously, resulting in a steep decrease in the measured current, marking their transit time. Positive ions are created in small number close to the photocathode with correspondingly short arrival times (traveling "back" to the cathode), and are not observable.

The arrival of two negative ion species of different mobilities is observed. The relative abundance of these two species is apparently dependent on (E/N): at $800\,$Td, the signal amplitude suggests a roughly equal number of both species, while at $550\,$Td the

slower ion species is barely visible. This is plausible if the slower ion is formed in a dissociative attachment process, requiring a certain electron energy which is more abundantly available at higher (E/N). The fact that the arrival of both anions results in sharp drops of the current implies that their lifetime with respect to electron detachment is at least greater than several ten μs at $3\,$kPa.

3.2. Evidence for a third, short-lived anion M_3^-

In measurements above $900\,$Td and below a few hundred Pa there is evidence for a third negative ion species, which detaches comparably quickly. Figure 2a shows an example, where the current waveform features a discontinuity in the steepness of the current at $5\,\mu$s. Although this feature appears to be weak, it is present in all waveforms, and corresponds to a physically consistent increase of the detachment rate coefficient with increasing (E/N). The observation of this third ionic species, which we denote M_3^-, is indirect: the drift of this ion does not contribute significantly to the current because it is very short-lived, but it results in a significant current from detached electrons.

### 3.3. Evidence for slow electron detachment from M_1^-

Above $900\,$Td and at high pressures above few kPa, the measured current shapes, as for instance shown in figure 2b, suggest an additional electron detachment process occurring on a longer timescale. From comparing the drift velocities it becomes apparent that this is the detachment signal of the slowest anion M_1^-. The obtained detachment rate coefficient ν_{d^1}/N of anion M_1^- is roughly three orders of magnitude lower than the one obtained for anion M_3^-, ν_{d^3}/N.

3.4. The positive ion M^+

Electron impact ionization of C_4F_7N creates at least one positive ion M^+. Distinguishing between different ionization channels and positive ions is not possible within the accuracy of our data. It is likely that the most abundant positive ion, denoted here as M^+, is $C_4F_7N^+$ since the parent ion is usually the dominating cation in discharges at mean electron energies of a few electronvolts. This might, however, not be the case for C_4F_7N since the considered (E/N) values and electron energies are high.

3.5. Electron and ion mobilities

The mobilities of M_1^- and M_2^- could be obtained from the arrival times as depicted in figure 1a, and increase with increasing electrical field strength. Figure 4 gives fits to the observed mobilities. Mobilities are
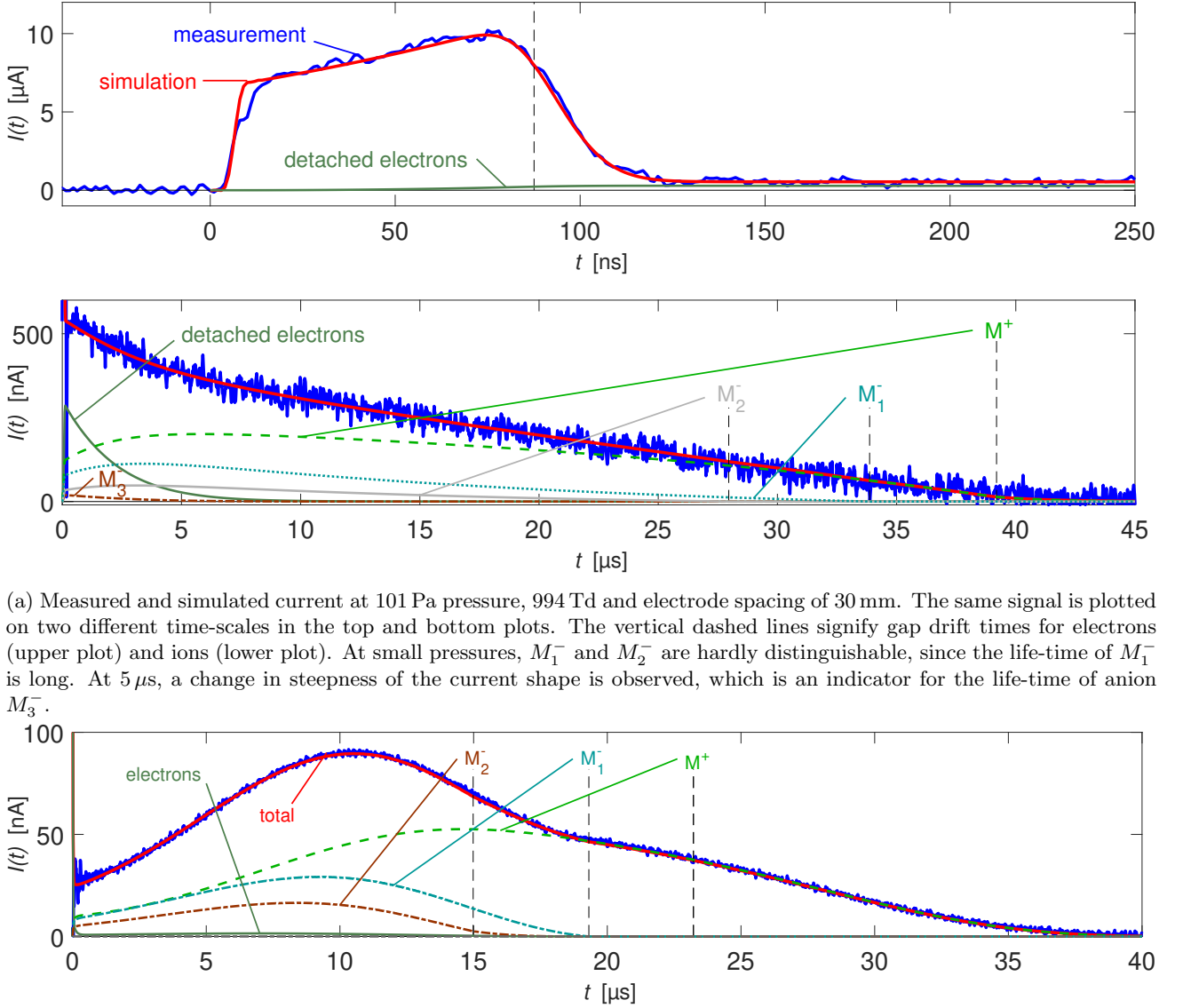
(a) Measured and simulated current at 101 Pa pressure, 994 Td and electrode spacing of 30 mm. The same signal is plotted on two different time-scales in the top and bottom plots. The vertical dashed lines signify gap drift times for electrons (upper plot) and ions (lower plot). At small pressures, M_1^- and M_2^- are hardly distinguishable, since the life-time of M_1^- is long. At $5\,\mu$s, a change in steepness of the current shape is observed, which is an indicator for the life-time of anion M_3^-.

(b) Measured and simulated current at 3020 Pa pressure, 948 Td and gap distance of 15 mm. The initial "electron-dominated" current is in this case too fast (a few nanoseconds) to be observable. The contributions of M_1^-, M_2^- and M^+ to the simulated current are plotted. M_3^- is not observable at this elevated pressures due to its very short lifetime, and is therefore omitted in the plot.

Figure 2

given in units $\mathrm{m^{-1}V^{-1}s^{-1}}$ such that $w = \mu N \cdot (E/N)$, where N is the gas number density at room temperature and w is the drift velocity of the respective species. The positive ion M^+ has a mobility of $\mu N = (7 \pm 1) \cdot 10^{20}\,\mathrm{m^{-1}V^{-1}s^{-1}}$, which could be obtained only above 950 Td, and with large uncertainty. Since M_3^- features fast electron detachment its mobility could not be determined, since the anion itself does not visibly influence the current shape.

For electrons, we use our previously derived mobility and longitudinal diffusion [10] in the fitting process.

3.6. Complete model and associated equations

These measurements motivate the following model with three negative ion species of different velocities w, represented in figure 3. The partial differential equations for the electron and ion densities $\rho(x,t)$ read:

$$\frac{\partial}{\partial t}\begin{pmatrix}\rho^{\mathrm{e}}(x,t)\\\rho^{M^+}(x,t)\\\rho^{M_1^-}(x,t)\\\rho^{M_2^-}(x,t)\\\rho^{M_3^-}(x,t)\end{pmatrix} + \begin{pmatrix}w^{\mathrm{e}}\\w^{M^+}\\w^{M_1^-}\\w^{M_2^-}\\w^{M_3^-}\end{pmatrix}\frac{\partial}{\partial x}\begin{pmatrix}\rho^{\mathrm{e}}(x,t)\\\rho^{M^+}(x,t)\\\rho^{M_1^-}(x,t)\\\rho^{M_2^-}(x,t)\\\rho^{M_3^-}(x,t)\end{pmatrix} =$$
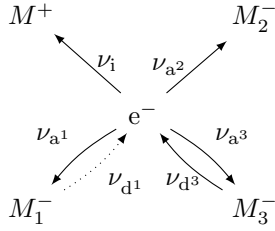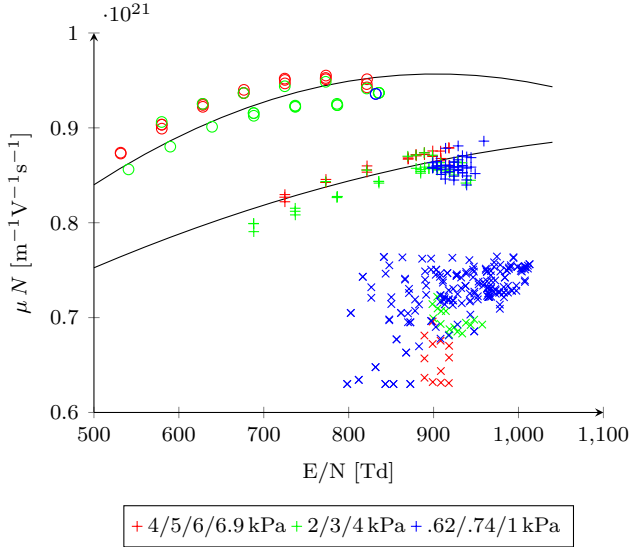
Figure 3: Model of electron and ion kinetics in C_4F_7N for (E/N) between 500 and 1050 Td. The dotted arrow signifies the low detachment rate ν_{d^1} from M_1^-.

| + 4/5/6/6.9 kPa | + 2/3/4 kPa | + .62/.74/1 kPa |

Marker-coded mobilities of ions (x positive ions, circles M_2^-, plus M_1^-).

Ion	$a \cdot 10^{14}$	$b \cdot 10^{17}$	$c \cdot 10^{20}$	conf. range
M^+	0	0	7	$950 - 1020$
M_1^-	-2.5	6.3	5.0	$650 - 920$
M_2^-	-7.2	13.0	3.7	$500 - 850$

(a) Ion mobilities at room temperature (unscaled) according to $\mu N = (a \cdot x^2 + b \cdot x + c)\,\mathrm{m^{-1}V^{-1}s^{-1}}$ with $x = (E/N)$ expressed in Td. The (E/N) range from which the values were deduced is indicated in the last column. The confidence is generally very low for the positive ion, and the mobility of the fast detaching ion M_3^- could not be established.

Figure 4

$$\begin{pmatrix} \nu_i - \nu_{a^1} \ldots \\ -\nu_{a^2} - \nu_{a^3} & 0 & \nu_{d^1} & 0 & \nu_{d^3} \\ \nu_i & 0 & 0 & 0 & 0 \\ \nu_{a^1} & 0 & -\nu_{d^1} & 0 & 0 \\ \nu_{a^2} & 0 & 0 & 0 & 0 \\ \nu_{a^3} & 0 & 0 & 0 & -\nu_{d^3} \end{pmatrix} \begin{pmatrix} \rho^e(x,t) \\ \rho^{M^+}(x,t) \\ \rho^{M_1^-}(x,t) \\ \rho^{M_2^-}(x,t) \\ \rho^{M_3^-}(x,t) \end{pmatrix}$$
$$(1)$$

4. Results

4.1. Ionization rate coefficient

The ionization rate coefficient, figure 5a, can be obtained best above 950 Td, and at low pressures. Taking detachment of ions into account yields values at $(55 \pm 10)\%$ of the value of our previous publication [10]. We will denote this scaling factor by $\kappa = 0.55$ in the following. Outside this range, no solutions are found that would reproduce the shape of the electron and ion current simultaneously.

At lower (E/N) or higher pressures the spread is strongly increased, and the optimization solution is seemingly no longer unique. We therefore must make an assumption on the shape of the ionization rate coefficients. Comparing to simulations in the well-known gas SF_6 (MAGBOLTZ [16]), and our previous results, we may assume that ν_i/N is approximated by an exponential function $a \exp(b \cdot (E/N))$. We assume further that the steepness of our previous results in this log-plot is a good approximation, which then yields the black dashed ($\kappa = 0.55$) and dotted lines ($\kappa = \{0.45, 0.65\}$). We evaluate all other rate coefficients for fixed ionization rate coefficient with $\kappa = \{0.45, 0.55, 0.65\}$ ("optimistic", "most likely", "pessimistic") and discuss the results in section 5.
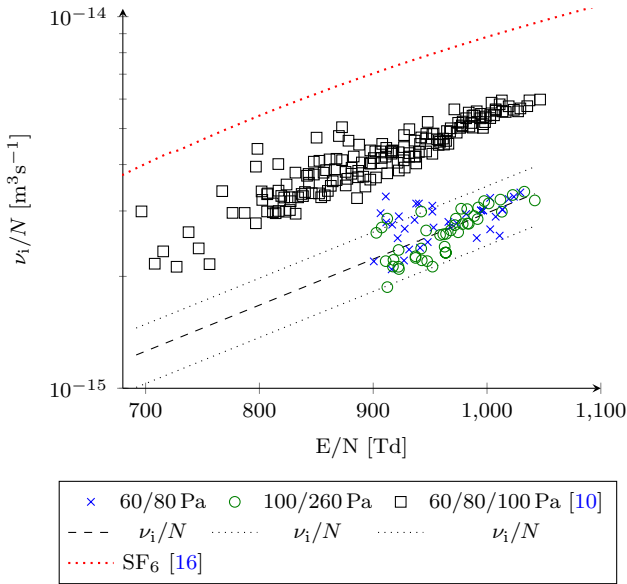
4.2. Attachment rate coefficients to M1 and M2

In figure 5b, the three independently fitted attachment rate coefficients are added up. When fixing the values of ν_i/N in the way described above, a very low spread in this sum of attachment rate coefficients is obtained. If ν_i/N is fitted, the spread is strongly increased. The resulting attachment rate coefficient shows an overall decreasing trend in (E/N), in contrast to the constant value obtained in our earlier publication [10], and is smaller in magnitude. Slightly higher or lower choices of ν_i/N, i.e. $\kappa = 0.45$ and 0.65, shift the sum of attachment rate coefficients accordingly.

In figure 1b the ratio of attachment to ion M_1^- and M_2^- was established (without making assumptions on ν_i/N), up to 850 Td, above which the spread increases strongly. Combining these results, we estimate ν_{a^1}/N and ν_{a^2}/N as shown in figure 5b in a high pressure limit ($\nu_{a^3}/N \approx 0$, see figure 7a). The dotted lines indicate hereby the lack of confidence in the extrapolation of the figure 1b above 850 Td.

4.3. Electron detachment from M1-

The electron detachment rate coefficient ν_{d^1}/N of M_1^-, figure 6, is increasing with increasing (E/N), and is seemingly independent of pressure. The rate is best derived from high pressure measurements at $2 - 6.9$ kPa, where the number of detachment events is sufficiently
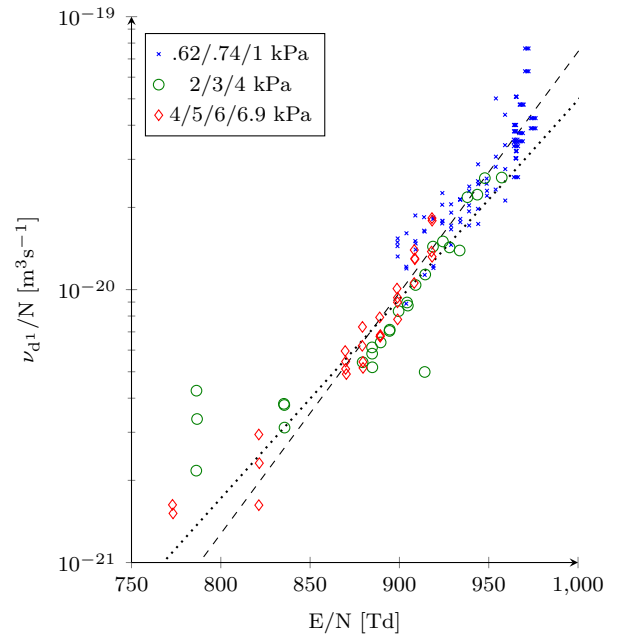
(a) The fitted ionization rate coefficient for small pressures $< 510\,\mathrm{Pa}$ and above $900\,\mathrm{Td}$, compared to our recent results [10] and SF_6 [16]. The dashed line indicates the extrapolated ionization rate coefficient.
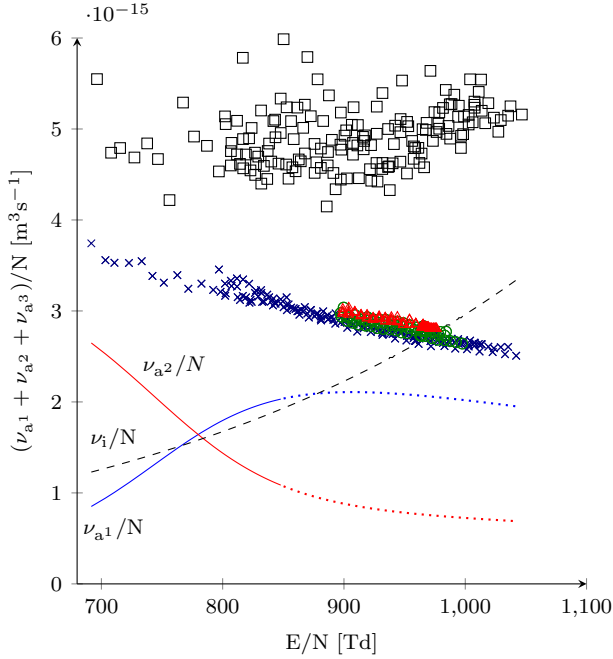
(b) The sum of attachment rate coefficients $(\nu_{a^1} + \nu_{a^2} + \nu_{a^3})/N$ in C_4F_7N, compared to our recent results. The values were obtained from measurements up to $1\,\mathrm{kPa}$.

Figure 5

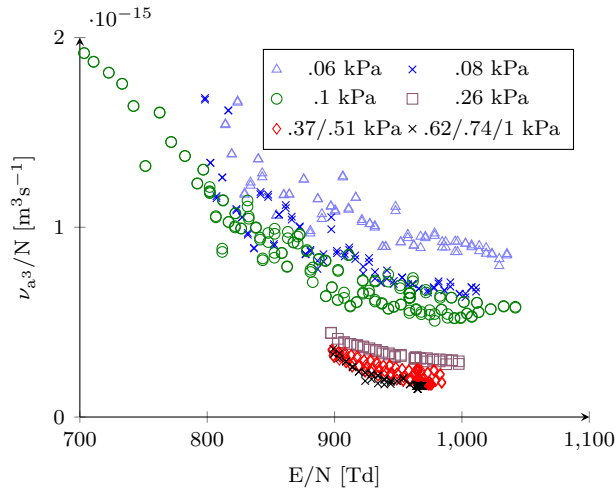The detachment rate coefficient of anion M_1^-, determined from measurements at $0.6 - 6.9\,\mathrm{kPa}$.

Figure 6

high to be well observable. Not keeping ν_i/N fixed does not influence the results for pressures above $2\,\mathrm{kPa}$ much, yet increases the spread for results at lower pressures. We obtain, with respect to $(E/N) < 900\,\mathrm{Td}$, optimistic (dashed) and pessimistic (dotted) fits as shown in the figure.

4.4. Short-lived anion

The attachment rate coefficient to M_3^- is plotted in figure 7a. The signature of detaching M_3^-, allowing the estimation of its attachment rate, can only be observed at small pressures below $1\,\mathrm{kPa}$. The obtained values of ν_{a^3}/N seemingly depend on the gas pressure, with smaller pressures corresponding to a higher value of ν_{a^3}/N, and decrease for increasing (E/N). Whether or not we fix ν_i/N does influence the spread of the results, but not the observed pressure dependency.

The rate ν_{d^3}/N of electron detachment from M_3^-, shown in figure 7b, is increasing with increasing (E/N), which is an important consistency check for detachment rates (at the onset of detachment). It is found to be slightly higher for higher pressures. The pressure dependencies of the attachment and detachment rate coefficients hint at a model deficiency, which we will discuss in section 5.

(a) The attachment rate coefficient to M_3^-, color and marker coded for different pressures.
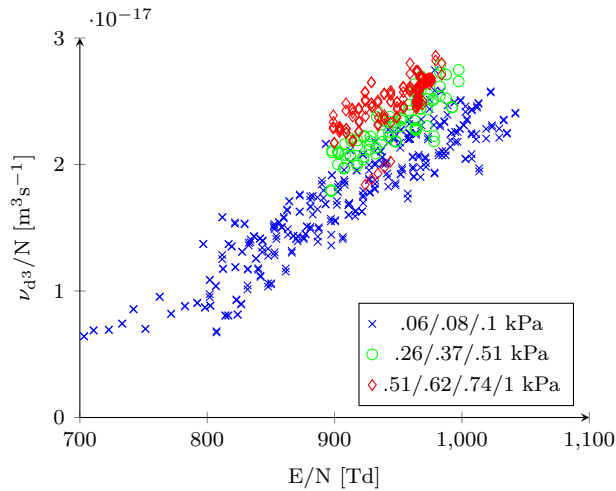

(b) The detachment rate coefficient of anion M_3^-, determined from measurements below 1000 Pa.

Figure 7

4.5. Density-reduced critical electric field $(E/N)crit$

Evaluating a "critical field strength" $(E/N)^*_{\text{crit}}$ in gases that show electron detachment from negative ions is a matter of definition. Commonly, it is defined as the (E/N) at which the ionization rate equals the attachment rate. In order to take detachment of electrons into account, we proposed [17] to redefine ν^*_{eff} as the largest eigenvalue of the system matrix of eq.(1): With $\vec{n}(x,t)$ being the number of species integrated over the gap,

$$\vec{n}(t) = \int_0^d \vec{\rho}(x,t)\mathrm{d}x \qquad (2)$$
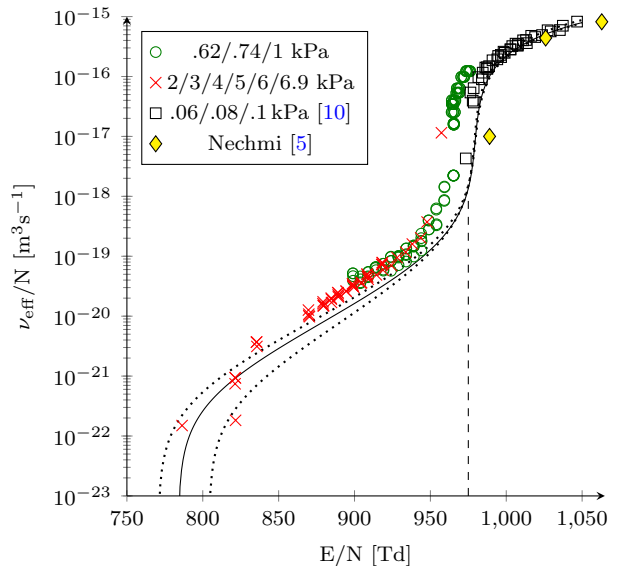
The effective ionization rate coefficient ν^*_{eff}/N of measurements at pressures above $0.6\,\text{kPa}$ is shown, as well as a high pressure limit calculation (black line) based on interpolated rate coefficients. Our previous results [10] (black squares) become negative below 975 Td (vertical dashed line). Results of Nechmi et al. [5] are given in yellow diamonds.

Figure 8

a direct solution without boundary effects (infinite electrode spacing) is given as

$$\vec{n}(t) = e^{M\,t}\vec{n}(0) \qquad (3)$$

where M is the system matrix of eq.(1). If at least one eigenvalue of M is positive, the exponential grows and describes a growing number of species $n(t)$. We therefore set ν^*_{eff} as the largest eigenvalue of M. This definition recovers $\nu_{\text{eff}} = \nu_i - \nu_a$ for zero detachment. Since the ν_{a^3}/N is seemingly decreasing with increasing pressure, we may neglect M_3^- as a high pressure limit. Then there exists a closed form [11] for this model for the effective ionization rate which can be stated as

$$\nu^*_{\text{eff}} = \tfrac{1}{2}(\nu_i - \nu_{a^2} - \nu_{a^1} - \nu_{d^1}) + \tfrac{1}{2}\sqrt{(\nu_i - \nu_{a^2} - \nu_{a^1} - \nu_{d^1})^2 + 4(\nu_i - \nu_{a^2})\nu_{d^1}} \qquad (4)$$

Figure 8 shows ν^*_{eff}/N, calculated according to eq. 4, for measurements above $620\,\text{Pa}$ and compares to our previous results [10]. Those were defined as ionization minus attachment, and become negative below 975 Td. The present values of ν^*_{eff}/N, on the other hand, are positive, i.e. overcritical, far below 975 Td. It is interesting to see that the effective ionization rate coefficients obtained with these two different definitions are in good agreement above 975 Td. Apart from a slightly higher scatter, ν^*_{eff}/N remains unchanged whether we fix ν_i/N or not.
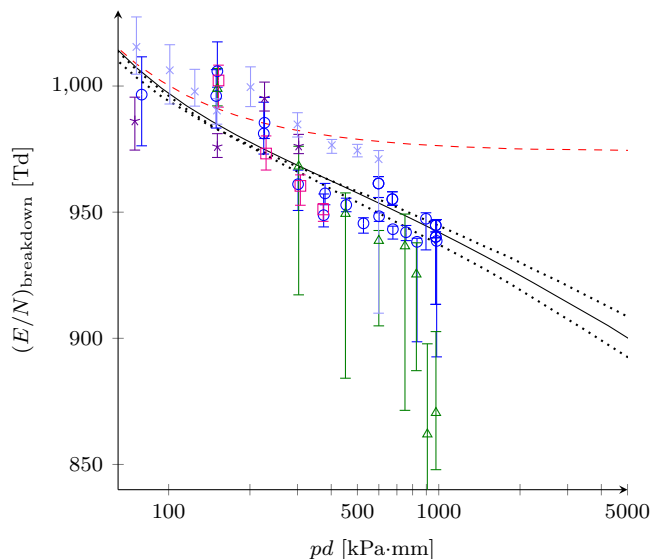
The $(E/N)_{bd}$ prediction in C_4F_7N, i.e. streamer criterion, calculated according to the model presented in this publication ("B", black, dotted and solid lines: see text) is compared to a streamer criterion "A" calculation according to the values of our previous publication, and experimental data from a breakdown experiment (marker: median voltage; error bars: 84% and 16% quartile; estimated systematic error of $3.5-5\%$ is not shown; unless otherwise noted, the distance is 15 mm.).

Figure 9

Inter- and extrapolating ν_i/N, ν_{a^1}/N, ν_{a^2}/N and ν_{d^1}/N for $\kappa = 0.55$ and calculating ν_{eff}/N yields the solid black line. Due to assuming $\nu_{a^3}/N \approx 0$ in a high-pressure limit, the calculated ν_{eff}/N deviates slightly from the measured data. Taking a lower ionization rate coefficient, i.e. $\kappa = 0.45$ and a more "optimistic" fit of ν_{d^1}/N (dashed line of figure 6) yields slightly lower ν_{eff}^*/N, and accordingly $\kappa = 0.65$ a slightly higher ν_{eff}^*/N, both shown as dotted lines in figure 8.

The calculated ν_{eff}^*/N becomes negative at $770 - 800$ Td, which is the theoretical $(E/N)_{crit}^*$.

4.6. Streamer criterion

A reduced electric field strength above $(E/N)_{crit}^*$ is a necessary, but not sufficient criterion for electric breakdown in homogeneous fields. A common way to predict the breakdown strength $(E/N)_{bd} > (E/N)_{crit}^*$ of a gas is to apply the streamer criterion [18, 19, 20]. In its simplest form, it states that $(E/N)_{bd}$ is reached when an avalanche grows strongly enough to reach a number
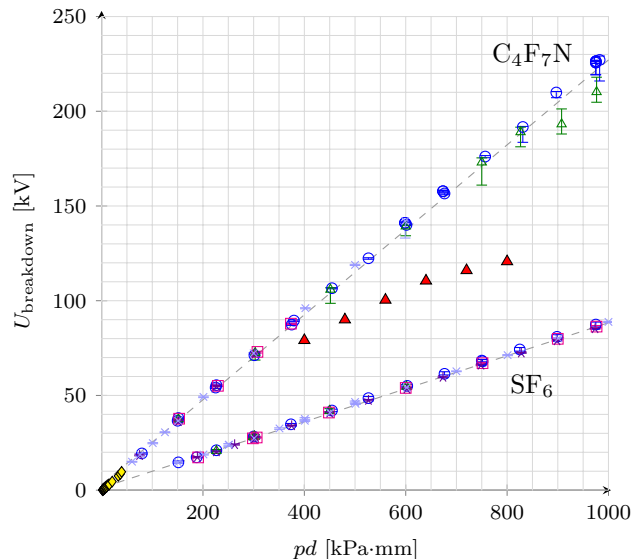
(a) Breakdown voltages of C_4F_7N and SF_6, plotted against pd, for polished and sandblasted electrodes. Unless otherwise noted, the distance is 15 mm. The error bars give the 84% and 16% percentile. A linear fit yields 360.8 ± 5 Td for SF_6 (offset of 1.3 kV). In yellow diamonds and red triangles the results of Nechmi et al. [5] and Zhang et al. [6] (4 mm) are given.
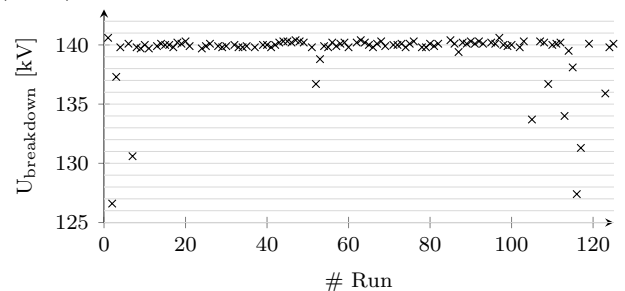
(b) 125 breakdown voltages measured in C_4F_7N at a pressure of 40 kPa and 15 mm gap distance. We used polished electrodes and $0.1 - 0.2$kV/s voltage increase rate.

Figure 10

of electrons N_e, in the order of $N_e = 10^8$. Then the discharge is assumed to be self-enhancing due to increase of the electric field by space charge effects (and potentially other mechanisms). This criterion was convincingly applied for instance in N_2 (appendix figure 2, from [14]).

For homogeneous fields it holds for both detaching and non-detaching gases that $(E/N)_{bd}$ converges to $(E/N)_{crit}^*$ at large pd, i.e. pressure times distance, since the growth of electrons scales exponentially with

pd. For lower pd, and in particular for detaching gases, corrections have to be applied in order to compare directly with breakdown results.

In non-detaching gases the streamer head is locally concentrated, making the electric field distortion particularly strong. In detaching gases, this is no longer the case since the attachment rate coefficients are larger than the ionization rate coefficient at $(E/N)^*_{\mathrm{crit}}$. Rather, due to being captured and statistically detached, electrons become smeared out over a larger volume. Therefore, space charge effects are presumably less pronounced. The streamer criterion should nevertheless give an approximate value of $(E/N)_{\mathrm{bd}}$.

In this context it is important to note that the effective velocity of electrons in a detaching gas may be orders of magnitudes smaller than the drift velocity of free electrons, due to the electrons being constantly attached and detached. Therefore, the relation between the effective growth per distance, usually denoted as α_{eff}, and the effective ionization rate ν^*_{eff} is not trivial. For the estimation of $(E/N)_{\mathrm{bd}}$ in C_4F_7N we simulate an avalanche with one start electron and a gap distance of 15 mm using the obtained rate coefficients. $(E/N)_{\mathrm{bd}}$ is defined as the lowest (E/N) for which $N_{\mathrm{e}} = 10^8$ electrons appear simultaneously in the gap.

We obtain the black line ("most likely"), and the dotted lines ("best" and "worst" case), denoted as "Criterion B" in figure 9, and find a slowly decreasing breakdown strength with increasing pd.

Choosing a different order of magnitude for the required electron multiplication than $N_{\mathrm{e}} = 10^8$ results in small shifts of $(E/N)_{\mathrm{bd}}$, and has almost no effect on the steepness of the curve. We try for instance $N_{\mathrm{e}} = 10^{10}$, which increases the values by less than 10 Td above $pd = 100\,\mathrm{kPa\cdot mm}$ (1 bar mm).

The "classical" streamer model using the obtained effective ionization rate coefficients of our previous publication as ionization minus attachment, is given by the red dashed line ("Criterion A"). This line approaches the critical field strength by classical definition, 975 Td.

4.7. Breakdown results

We compare $(E/N)_{\mathrm{bd}}$ to AC voltage rise tests. In figure 10b, an example of a typical sequence of 125 breakdowns is shown, and figure 10a gives the obtained breakdown voltage for pd up to 1000 kPa·mm, for both sandblasted and polished electrodes. The median is given by the marker, while the error bars give the 84% and 16% percentiles. As a reference for this setup, results for SF_6 are shown for which a linear fit (dashed line) yields 360.8 ± 5 Td (offset of 1.3 kV). For C_4F_7N a similar fit gives 933.0 ± 12 Td (offset of 2.9 kV; excluding outliers). However, this ansatz assumes a pressure independent electric strength, which is

presumably not the case for C_4F_7N.

Contrary to SF_6, in C_4F_7N soot formation was found to have significant influence and made measurements at high pd challenging. After $50 - 200$ breakdowns, a significant drop of the breakdown voltage was observed, by up to 30% of the initial values (see figure 10b). This effect is stronger for higher voltage. Therefore, the electrodes were frequently cleaned.

In figure 9 the breakdown voltages are given in units of (E/N), using different markers and colors for different experimental conditions. The agreement between $(E/N)_{\mathrm{bd}}$ and the measured values is good for polished electrodes over the entire measured pd range. Above $800\,\mathrm{kPa\cdot mm}$, the median voltages for sandblasted electrodes diverge and we obtain lower values than predicted. Values of Nechmi et al. [5] measured the breakdown strength for pd up to $\approx 40\,\mathrm{kPa\cdot mm}$. At these pd, the correction from the streamer mechanism is dominating, and their values in units of Td are much higher than ours. An extrapolation to higher pd yields 982 Td, which matches well with our criterion "A". Zhang et al. [6] obtain values in between 800 Td at $400\mathrm{kPa\cdot mm}$ and 620 Td at $800\,\mathrm{kPa\cdot mm}$ at a distance of 4 mm.

5. Discussion

5.1. Kinetic model

Discharges in gases that exhibit electron detachment are difficult to model. For the case of C_4F_7N we attempt to set up an appropriate ion kinetic model ab initio, based on measurements at different electric fields and pressures. Having observed different mobilities of two negative ions and the characteristic current shapes of a further, fast detaching anion, we distinguish three anions in C_4F_7N. The measured current shapes are then fitted with respect to the underlying rate equations. The presented model reproduces all measured currents at different pressures from $60 - 7900\,\mathrm{Pa}$ and (E/N) in between 500 and 1050 Td.

However, it is certainly only an approximation to the real physical discharge: Pressure dependencies in the rate coefficients for ion M_3^- hint at processes that are not described within our model. A plausible scenario could be that the fast-detaching M_3^- undergoes a form of collisional ion conversion towards a more stable species M_1^- or M_2^-. When this conversion rate becomes faster at higher pressures, more stable ions such as M_1^- or M_2^- are "observed" in our fitting procedure, and the relative amount of M_3^- is decreasing. This would agree with our results, seeing that the sum of attachment rate coefficients is almost pressure independent. Therefore it is likely that the physical, "undisturbed" rate coefficient ν_{a^3}/N lies above our obtained

values. The low pressure limit of our results suggests values larger than $2 \cdot 10^{-15} \mathrm{m^3 s^{-1}}$, with large uncertainty.

Within the accuracy of our setup, we are unable to investigate this effect further, but these details are fortunately not important for the estimation of $(E/N)^*_{\mathrm{crit}}$ at elevated pressures above $1 \,\mathrm{kPa}$. Since the detachment rate coefficient $\nu_{\mathrm{d^3}}/N$ is very high, and the attachment rate coefficient $\nu_{\mathrm{a^3}}/N$ diminishes with increasing pressure, anion M_3^- may be neglected.

5.2. Identification of the anions

Current measurements at high pressures and low (E/N) allowed an estimation of the ratio of attachment to the long-lived ions M_1^- and M_2^-, shown in figure 1b. The ratio is seen to shift strongly towards M_1^- with increasing (E/N). The formation of the anion M_1^- is therefore presumably a dissociative attachment process at higher energy than M_2^-. With increasing (E/N), the average electron energy increases and makes attachment to M_1^- with its higher energy threshold more likely than attachment to M_2^-. This should allow the identification of the ion species in comparison to experiments from which attachment cross sections can directly be derived.

Collisional detachment requires that an anion gains enough internal energy to overcome the electron detachment threshold. Consequently, the highly different detachment rates presumably indicate anions of different electron affinity. M_1^- and M_2^- should have quite high affinities, which indicates ions like F^- or CN^-. Various other ions might show the behaviour of M_3^-, like $C_x F_y^-$ or the parent anion $C_4 F_7 N^-$.

5.3. Correction of ionization and attachment rate coefficient

The present results suggest a down-correction of the ionization rate coefficient by $\approx 45\%$ with respect to our previous results [10]. The total attachment rate coefficient, on the other hand, seems to be only $20 - 40\%$ smaller. The ionization rate coefficient from our last publication was obtained under the assumption that the lifetime of negative ions is far larger than the transit time to the anode, at pressures below $100 \,\mathrm{Pa}$. It turns out not to be the case for the fastest detaching ion M_3^- at $100 \,\mathrm{Pa}$ and above $950 \,\mathrm{Td}$, where it has, according to the present results, a lifetime of about $2 \,\mu s$. It would therefore almost certainly detach over the drift time of $15 - 30 \,\mu s$ (at $1 - 2 \,\mathrm{cm}$ gap distance). Furthermore, its apparent attachment rate coefficient $\nu_{\mathrm{a^3}}/N$ is increasing with decreasing pressures. Therefore, our previous evaluation overestimated the values for the ionization and attachment rates.

5.4. Electric breakdown strength estimation

The example waveform 2b at $3020 \,\mathrm{Pa}$ and $948 \,\mathrm{Td}$ gives a clear indication that $(E/N)^*_{\mathrm{crit}}$ is presumably lower than $948 \,\mathrm{Td}$. Although the ionization rate coefficient is smaller than the sum of attachment rate coefficients, the current is visibly growing over time.

A theoretical $(E/N)^*_{\mathrm{crit}}$ of $785 \pm 15 \,\mathrm{Td}$ was obtained in section 4.5. However, the small magnitude of ν^*_{eff}/N in the range below $900 \,\mathrm{Td}$ of figure 8 let the question arise whether this rate coefficient may just be too small to effectively initiate an avalanche with sufficient electron growth in a gas to lead to a breakdown. A streamer simulation confirmed this: The difference between the breakdown strength and the theoretical $(E/N)^*_{\mathrm{crit}}$ can be huge for application-relevant voltages and pd. At relatively large $pd = 5000 \,\mathrm{kPa \cdot mm}$, we estimate the breakdown strength at around $900 \,\mathrm{Td}$, or over $U = 10^6 \,\mathrm{V}$, far above $(E/N)^*_{\mathrm{crit}}$.

5.5. Breakdown results

We compare $(E/N)_{\mathrm{bd}}$ to measured breakdown voltages for pd up to $1000 \,\mathrm{kPa \cdot mm}$, using polished and sandblasted electrodes in a uniform field configuration. Up to pd of $1000 \,\mathrm{kPa \cdot mm}$ and polished electrodes, $C_4 F_7 N$ has a higher electric strength than SF_6 by a factor of 2.6. The results agree well with the predicted $(E/N)_{\mathrm{bd}}$, and follow the decreasing trend with increasing pd, which stems from slow electron detachment in our model. However, roughness effects would show a very similar trend, and we cannot fully exclude its influence. We try to test this by comparing polished and roughened ($R_t = 13 \,\mu m$) electrodes: judging from the median breakdown voltages of figure 10a, there is no significant difference up to $pd = 800 \,\mathrm{kPa \cdot mm}$. Nevertheless, the predicted decrease in $(E/N)_{\mathrm{bd}}$ is, for measurable pd and homogeneous fields, too small to clearly attribute it to electron detachment alone.

5.6. Gas mixtures with C4F7N

$C_4 F_7 N$ is considered for application as electrical insulation gas mainly in mixtures with CO_2 and O_2. Typical mole fractions of $C_4 F_7 N$ are $5 - 7\%$, with corresponding lower critical field strength of $210 - 260 \,\mathrm{Td}$ [10]. Since average electron and ion energies at these fields are lower, the results for pure $C_4 F_7 N$ of this publication can presumably not be transferred directly. M_1^- might not be created in large amounts, and would presumably not show electron detachment. The rather

weak electron detachment signals that we observed in preliminary measurements in those mixtures might stem from M_3^-.

Conclusion

Within this work, we have found evidence for three negative ions in C_4F_7N discharges, which may be identified in future by comparison with experiments that allow the direct identification of the ionic species. We obtained the magnitude of the attachment rates to these anions as a function of (E/N), and proposed a kinetic model. However, the understanding of C_4F_7N remains incomplete until partial attachment cross sections are measured.

Electron detachment has implications on the electric strength of the gas: we calculate that the density-reduced critical electric field strength lies between 785 ± 15 Td and is $175 - 205$ Td lower than values that were proposed previously [5, 10]. Our results demonstrate the need to distinguish between anions in cases where electron detachment occurs, since, in the limit of high pd detaching anions do not contribute to the electric strength of a compound. In uniform electric fields, a simple streamer criterion, using our proposed model, yields a good estimate of the breakdown strength of the gas. We showed further that the estimated breakdown strength $(E/N)_{\mathrm{bd}}$ converges to the theoretical critical field strength $(E/N)_{\mathrm{crit}}^*$ only very slowly with increasing pd. Comparing to breakdown measurements, we find good agreement between theory and experiment. Considering inhomogeneous electric fields, the electric strength of C_4F_7N might drop significantly: at high electric fields, the anionic composition changes and shifts towards the "weaker" anion M_1^-. Furthermore, electron detachment might stronger affect the discharge. This would explain why Zhang et al. [6] observed a weaker performance of C_4F_7N:CO_2 mixtures in non-homogeneous fields than expected. Simulations including anion detachment should be performed in various geometries in order to answer these questions and derive design recommendations.

Acknowledgments

References

[1] Costello M, Flynn R and Bulinski M 2013 Fluorinated nitriles as dielectric gases WO Patent App. PCT/US2013/031,854 URL https://encrypted.google.com/patents/WO2013151741A1?cl=en

[2] Kieffel Y, Girodet A, Biquez F, Ponchon P, Owens J, Costello M, Bulinski M, San R V and Werner K 2014 SF$_6$ alternative development for high voltage switchgears *Cigre, Paris* paper D1-305 URL https://e-cigre.org/publication/SESSION2014-2014-cigre-session-set-of-papers--proceedings

[3] Owens J G 2016 Greenhouse gas emission reductions through use of a sustainable alternative to sf6 *IEEE Electrical Insulation Conference (EIC), 2016* (IEEE) pp 535–538

[4] Christophorou L G and Olthoff J K 2000 *Journal of Physical and Chemical Reference Data* **29** 267–330 URL http://dx.doi.org/10.1063/1.1288407

[5] Nechmi H E, Beroual A, Girodet A and Vinson P 2017 *IEEE Transactions on Dielectrics and Electrical Insulation* **24** 886–892 ISSN 1070-9878 [Factor of 10 correction in the x axis of figure 4 confirmed in private communication.]

[6] Zhang B, Uzelac N and Cao Y 2018 *IEEE Transactions on Dielectrics and Electrical Insulation* **25** 1340–1350 ISSN 1070-9878 [distance of electrodes of figures 7/8 confirmed to be 4mm instead of 10mm in private communication with the authors]

[7] Li Y, Zhang X, Zhang J, Fu M, Zhuo R, Luo Y, Chen D and Xiao S 2018 *High Voltage*

[8] Nechmi H E, Beroual A, Girodet A and Vinson P 2016 *IEEE Transactions on Dielectrics and Electrical Insulation* **23** 2587–2593

[9] Wiener J, Hinrichsen V, Goll F and Juhre K 2017 *Proceedings of the 20th International Symposium on High Voltage Engineering* URL http://tubiblio.ulb.tu-darmstadt.de/89376/

[10] Chachereau A, Hösl A and Franck C M 2018 *Journal of Physics D, Applied Physics*

[11] Wen C and Wetzer J 1988 *IEEE transactions on electrical insulation* **23** 999–1008

[12] Haefliger P and Franck C M 2018 *Review of Scientific Instruments* **89** 023114

[13] Dahl D A, Teich T H and Franck C M 2012 *Journal of Physics D: Applied Physics* **45** 485201 URL http://stacks.iop.org/0022-3727/45/i=48/a=485201

[14] Haefliger P and Franck C 2018 *Journal of Physics D: Applied Physics* **52** 025204

[15] Hösl A, Häfliger P and Franck C M 2017 *Journal of Physics D: Applied Physics* **50** 485207

[16] Biagi S 1999 *Nuclear Instruments and Methods in Physics, Research Section A* **412** 234–240 URL http://dx.doi.org/10.1016/S0168-9002(98)01233-9

[17] Haefliger P, Hösl A and Franck C M 2018 *Journal of Physics D: Applied Physics* **51** 355201

[18] Meek J 1940 *Physical review* **57** 722

[19] Pedersen A, McAllister I, Crichton G and Vibholm S 1984 *Archiv für Elektrotechnik* **67** 395–402

[20] Lu X and Ostrikov K 2018 *Applied Physics Reviews* **5** 031102

[21] Dakin T, Luxa G, Oppermann G, Vigreux J, Wind G and Winkelnkemper H *Air, and Sulfur Hexafluoride, Electra* 61–82

[22] Biagi database, data extracted from the fortran program MAGBOLTZ of S.F. Biagi, versions 8.9 and after, data retrieved on April 19, 2017 URL www.lxcat.net/Biagi

[23] Hagelaar G and Pitchford L 2005 *Plasma Sources Science and Technology* **14** 722–733 ISSN 0963-0252 URL http://dx.doi.org/10.1088/0963-0252/14/4/011
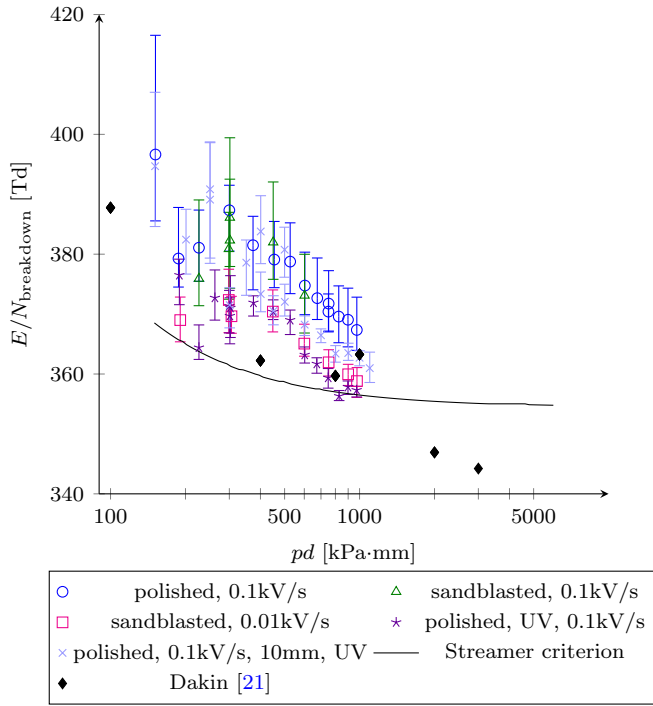
Appendix

Figure 1: SF$_6$ breakdown measurements, compared to reference data (Dakin [21]). Cross section data from [22] and Bolsig+ [23] was used to calculate the streamer criterion with $N_e = 10^8$.
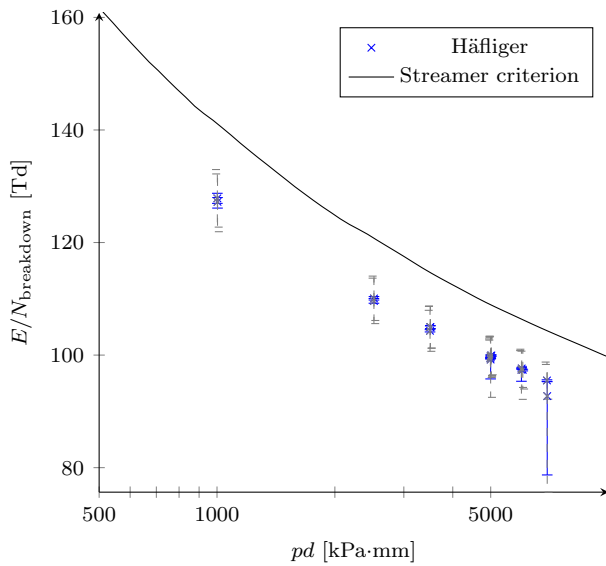

Figure 2: Breakdown measurements in pure N$_2$, taken from [14], compared to a streamer criterion calculation using an electron number of $N_e = 10^8$. Cross section data from [22] and Bolsig+ [23] was used to calculate the streamer criterion.